molecular pharmaceutics

Article

pubs.acs.org/molecularpharmaceutics

Re-Engineered p53 Chimera with Enhanced Homo-Oligomerization That Maintains Tumor Suppressor Activity

Abood Okal,[†] Sean Cornillie,[‡] Stephan J. Matissek,[§] Karina J. Matissek,[†,∥] Thomas E. Cheatham, III,[‡] and Carol S. Lim*[,†]

[†]Department of Pharmaceutics and Pharmaceutical Chemistry, University of Utah, Salt Lake City, Utah 84112, United States

[‡]Department of Medicinal Chemistry, University of Utah, Salt Lake City, Utah 84112, United States

[§]Faculty of Biotechnology, Biberach University of Applied Sciences, 88400 Biberach, Germany

[∥]Department of Pharmaceutics and Biopharmacy, Philipps-Universität, D-35032 Marburg, Germany

Supporting Information

ABSTRACT: The use of the tumor suppressor p53 for gene therapy of cancer is limited by the dominant negative inactivating effect of mutant endogenous p53 in cancer cells. We have shown previously that swapping the tetramerization domain (TD) of p53 with the coiled-coil (CC) from Bcr allows for our chimeric p53 (p53-CC) to evade hetero-oligomerization with endogenous mutant p53. This enhances the utility of this construct, p53-CC, for cancer gene therapy. Because domain swapping to create p53-CC could result in p53-CC interacting with endogenous Bcr, which is ubiquitous in cells, modifications on the CC domain are necessary to minimize potential interactions with Bcr. Hence, we investigated the possible design of mutations that will improve homodimerization of CC mutants and disfavor hetero-oligomerization with wild-type CC (CCwt), with the goal of minimizing potential interactions with endogenous Bcr in cells. This involved integrated computational and experimental approaches to rationally design an enhanced version of our chimeric p53-CC tumor suppressor. Indeed, the resulting lead candidate p53-CCmutE34K-R55E avoids binding to endogenous Bcr and retains p53 tumor suppressor activity. Specifically, p53-CCmutE34K-R55E exhibits potent apoptotic activity in a variety of cancer cell lines, regardless of p53 status (in cells with mutant p53, wild-type p53, or p53-null cells). This construct overcomes the dominant negative effect limitation of wt p53 and has high significance for future gene therapy for treatment of cancers characterized by p53 dysfunction, which represent over half of all human cancers.

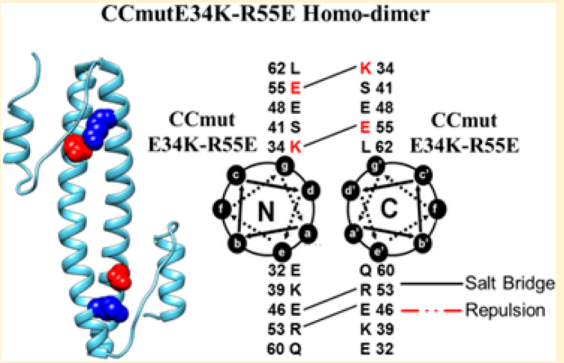

KEYWORDS: *p53, dominant-negative effect, tetramerization domain, coiled-coil, Bcr, breast cancer, tumor suppressor*

INTRODUCTION

The protein p53 is a tumor suppressor that acts as a transcription factor, which can activate multiple pathways such as DNA repair, cell cycle arrest, and apoptosis.[1−3] The tumor suppressor p53 is the most commonly mutated gene of all human cancers, making it an ideal therapeutic target.[4,5] Specifically, p53 is most frequently mutated in lung, head and neck, colon, ovarian, stomach, breast carcinomas, and many others.[6] Although current targeting of p53 as a therapeutic is mainly focused on introducing the wild-type (wt-p53) p53 gene into cancer cells using various delivery vehicles,[7−9] the diversity of p53 mutations precludes finding a single drug that hits all possible variants of the protein.[10]

In cancer cells, mutant p53 may not only impair tumor suppressor function and transcriptional activity but also effectively deplete wt-p53 because mutant p53 retains its ability to oligomerize with other p53 via the tetramerization domain (TD).[11,12] Upon hetero-oligomerization of mutant and wt-p53 in cancer cells, mutant p53 exerts a dominant negative effect over wt-p53 and leads to its inactivation.[13−15] To overcome these issues, our alternative approach has been to engineer a chimeric version of p53 for cancer gene therapy that can be used universally, regardless of p53 mutational status in cancer.[16] To create this chimeric, transcriptionally active version p53 that can only form homotetramers, we searched for possible domain swapping motifs and chose to replace the 31 amino acid TD of p53[17] with the 72 amino acid coiled-coil (CC) of Bcr (breakpoint cluster region protein).[18] Superficially, these motifs may appear structurally dissimilar, but both the TD and CC contain a main α helix that orients in an antiparallel fashion and forms a dimer of dimers.[17,18] Due to their similar orientation and ability to form tetramers, the CC motif from Bcr was a reasonable starting point for domain swapping. We have shown

Received: March 14, 2014
Revised: May 9, 2014
Accepted: May 16, 2014
Published: May 16, 2014

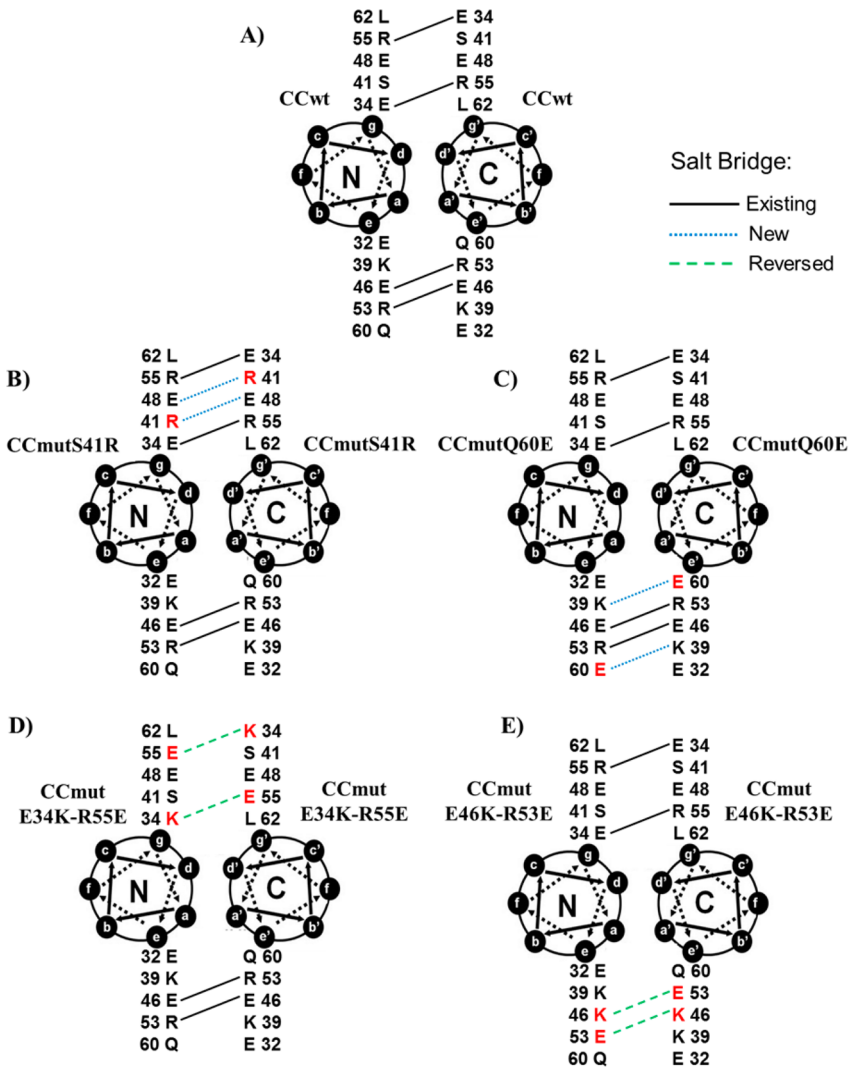

Figure 1. Helical wheel diagrams of wild-type CC homodimers (CCwt) (A), CCmutS41R homodimers (B), CCmutQ60E homodimers (C), CCmutE34K-R55E homodimers (D), and CCmutE46K-R53E homodimers (E). Solid lines indicate possible ionic interactions already existing in the wild-type coiled-coil. Dotted (blue) lines represent newly formed ionic interactions. Dashed (green) lines indicate reversed ionic interactions existing in the wild-type coiled-coil.

previously[16] that swapping the tetramerization domain of p53 with the CC domain enhances the utility of p53 for cancer gene therapy in p53-dominant negative breast cancer cells. This alteration of the oligomerization motif of the tumor suppressor allowed for our chimeric p53, namely, p53-CC, to evade hetero-oligomerization with endogenous mutant p53 commonly found in cancer cells while retaining the tumor suppressor function of p53. This proves to be critical since mutant p53 has a transdominant inhibitory effect over wild-type p53 upon hetero-oligomerization.

Bcr, from which the CC was obtained, is a ubiquitous eukaryotic phosphotransferase and has mostly been studied in the context of chronic myeloid leukemia (CML) where a reciprocal chromosomal translocation with Abl results in the fusion protein Bcr-Abl, the causative agent of CML.[19,20] Generally, Bcr may be involved in inflammatory pathways and cell proliferation.[21] Although it has been shown that Bcr-knockout mice still survive, one of the major defects in these mice was reduced intimal proliferation in low-flow carotid arteries compared to wild-type mice.[21] In addition, Bcr plays a role in arterial proliferative disease in vivo as well as differentiation and inflammatory responses of vascular smooth muscle cells.[22,23] Because domain swapping to create p53-CC could result in p53-CC interacting with endogenous Bcr, modifications on the CC domain are necessary to minimize potential interactions with Bcr. Hence, the purpose of this work is to modify the CC domain in p53-CC to reduce potential interactions with endogenous Bcr.

Coiled-coil domains are characterized by heptad repeats of amino acids (denoted by letters for each residue, $(\mathbf{abcdefg})_n$, for n repeats) that control the specificity and orientation of the oligomerization motif.[24,25] Distinct interaction profiles exist between the different residues based on the orientation (parallel or antiparallel) of the coiled-coil.[24,26] Surface interactions between positions **e** to **e**′ (where the ′ denotes a residue on the opposing α helix in the dimer) and **g** to **g**′ are known to be essential in antiparallel coiled-coils, whereas interactions between positions **g** to **e**′ are the most critical for parallel coiled-coils.[24,26] The coiled-coil domain from Bcr is assembled as two 36-residue helices antiparallel to each other (Figure 1A).[27,28] This antiparallel orientation gives rise to the aforementioned **e** to **e**′ and **g** to **g**′ interactions that can be

dx.doi.org/10.1021/mp500202p | *Mol. Pharmaceutics* 2014, 11, 2442−2452

utilized to potentially modify electrostatic interactions within a dimer. We investigated the possible design of mutations that will form opposing charges on residues **e** to **e′** and **g** to **g′** to increase salt bridge formation (see Figure 1) in order to improve homodimerization of CC mutants and disfavor hetero-oligomerization with wild-type (CCwt), with the goal of minimizing potential interactions with endogenous Bcr in cells. In silico examination of CCwt (Figure 1A) revealed that Bcr has uncharged Ser-41 at position **g** and Glu-48 (acidic) representing **g′** that are within proximity for salt bridge formation. Similarly, CCwt has uncharged Gln-60 at position **e** and Lys-39 (basic) at position **e′** which are also within proximity for salt bridge formation. Therefore, we hypothesized that introducing S41R (Arg, basic) and Q60E (Glu, acidic) mutations separately, would potentially form two extra salt bridges per mutation (Figure 1B and C, respectively). These two mutant candidates are referred to as CCmutS41R and CCmutQ60E.

In addition, examination of the coiled-coil interchain salt bridges indicate that two more potential compound mutants (i.e., more than one mutation per candidate) could be made to improve homodimerization of CC mutants. Mutation of Glu-34 to Lys and Arg-55 to Glu (CCmutE34K-R55E) will preserve all four stabilizing salt bridges found in CCwt in the case of CCmut homo-oligomerization (Figure 1D). However, in the case of CCmutE34K-R55E hetero-oligomerization with CCwt, only two stabilizing salt bridges are maintained while two destabilizing charge−charge repulsions are formed (further discussed in the results). This allows for increased specificity for CCmutE34K-R55E toward homo-oligomerization over hetero-oligomerization with CCwt. Similarly, introducing the E46K and R53E compound mutation (CCmutE46K-R53E) results in favoring homo-oligomerization (Figure 1E). Disfavoring hetero-oligomer formation with CCwt represents minimizing interactions with endogenous Bcr in cells.

The resulting designed four mutant candidates, p53-CCmutS41R, p53-CCmutQ60E, p53-CCmutE34K-R55E, and p53-CCmutE46K-R53E, are listed in Table 1 and were further assessed computationally and tested in vitro for their ability to retain apoptotic activity and minimize any possible interaction with endogenous Bcr.

Table 1. Mutant Candidates and the Rationale of the Design for Each Mutation

mutations CCmut	purpose	rationale	net ionic interactions
S41R	increase binding stability	two new salt bridges	6
Q60E	increase binding stability	two new salt bridges	6
E34K-R55E	increase binding specificity (homodimers)	reverse an existing salt bridge	4
E46K-R53E	increase binding specificity (homodimers)	reverse an existing salt bridge	4

MATERIALS AND METHODS

Computational Modeling and Simulation. Models of the Bcr CC domain were built starting with the crystal structure of the N-terminal oligomerization domain of Bcr-Abl (Protein Data Bank code 1K1F, choosing residues 1−67 in each of chains A and B). Using the *swapaa* tool in Chimera,[29] selenomethionine residues were reverted back to methionine and residue 38 was mutated back to cysteine, consistent with the wild-type structures. Models of the mutant coiled-coils were built using the *swapaa* tool, which facilitates placement of modified side chains by sourcing the Dunbrack backbone-dependent rotamer library to predict the most accurate side-chain rotamers.[30] Models were built using ff12SB[31,32] force field parameters and explicitly solvated in truncated octahedron with at least a 10 Å surrounding buffer of TIP3P water.[33] Net-neutralizing counterions (Na^+/Cl^-) were incorporated using the Joung and Cheatham ion parameters,[34] and 52 additional Na^+/Cl^- atoms were added to achieve an approximate ion concentration of 200 mM. All models were subjected to an extensive minimization and equilibration protocol to relax and steer systems toward energetically favored conformations prior to production molecular dynamics (MD). An initial minimization was performed (500 steps of steepest descent, 500 steps of conjugate gradient) prior to heating the system to 300 K. A 25 kcal/(mol Å^2) restraint was placed upon backbone C_α atoms throughout the initial minimization and heating step. Following the initial minimization and heating, systems were subjected to five cycles of minimization (500 steps of steepest descent, 500 steps of conjugate gradient) and equilibration, in which the restraint weights were lifted sequentially from 5 to 1 kcal/(mol Å^2) following each cycle. A final equilibration was performed for 500 ps with a restraint weight of 0.5 kcal/(mol Å^2) prior to production MD. Constant temperature (300 K) and pressure (1 bar) were controlled throughout the minimization protocol using a Berendsen thermostat[35] with a 0.2 coupling time. All production MD simulations were carried out with the AMBER 12.0 modeling code suite[36,37] for 200 ns (using a 2 fs time step) in explicit solvent, using a Langeven thermostat[38] with a collision frequency of 1 ps^{-1} to control constant temperature and pressure,[39] a 10 Å nonbonded cutoff, default particle mesh Ewald treatment of electrostatics,[40] and SHAKE applied to bonds to hydrogens.[41]

Analysis of the MD trajectories was performed using the ptraj and CPPTRAJ analysis tools[42] available in the AmberTools 12.0 and 13.0 distributions: RMSD and 2D-RMS analyses were employed to monitor if the protein structure retained the expected structure, and clustering analysis of the structures sampled during the MD (using the average linkage algorithm)[43] was used to identify the most frequently sampled protein conformations of each MD trajectory. Additionally, a DSSP analysis[44] of secondary structure was performed to determine the percent helicity of each mutant, and α-helical-specific hydrogen bonds were recorded by monitoring hydrogen bonding interactions between peptide backbone atoms of i and $i + 4$ residues. The atomic positional fluctuations of C_α backbone atoms were recorded to identify regions of flexibility in response to the induced mutations. An MM-PBSA energetic analysis was performed to assess the relative binding energies of each mutant.[45,46]

Cell Lines and Transient Transfections. T47D human ductal breast epithelial tumor cells (ATCC, Manassas, VA), COS-7 monkey kidney fibroblast cells (ATCC), SKOV-3.ip1 human ovarian adenocarcinoma cells (a kind gift from Dr. Margit Janát-Amsbury, University of Utah), and MCF-7 human breast adenocarcinoma cells (ATCC) were cultured in RPMI 1640 (T47D, COS-7, MCF-7) or DMEM (SKOV-3.ip1) (Invitrogen, Carlsbad, CA) supplemented with 10% FBS (Invitrogen), 1% penicillin-streptomycin (Invitrogen), 1% glutamine (Invitrogen) and 0.1% gentamycin (Invitrogen). Additionally, T47D and MCF-7 cells were supplemented with 4

mg/L insulin (Sigma, St. Louis, MO). Cells were maintained in a 5% CO_2 incubator at 37 °C. For all assays, 3.0×10^5 cells for T47D and MCF-7 cells, or 2.0×10^5 for COS-7 and SKOV-3.ip1 cells were seeded in 6-well plates (Greiner Bio-One, Monroe, NC). Approximately 24 h after seeding, transfection was performed using 1 pmol of DNA per well and Lipofectamine 2000 (Invitrogen) following the manufacturer's recommendations.

Plasmid Construction. The plasmids pEGFP-wt-p53 (wt-p53), pEGFP-p53-CC (p53-CCwt), and pEGFP-CC (CCwt) were subcloned as previously.[16,47] pEGFP-p53-CCmutS41R (p53-CCmutS41R), pEGFP-p53-CCmutQ60E (p53-CCmutQ60E), pEGFP-p53-CCmutE34K-R55E (p53-CCmut-E34K-R55E), and pEGFP-p53-CCmutE46K-R53E (p53-CCmutE46K-R53E) were created through site directed mutagenesis using pEGFP-p53-CC as the template.

The following primers were used for the p53-CCmutS41R mutation: 5′-ggagcgctgcaaggcccgctccattcggcgcctgg-3′ and 5′-ccaggcgccgaatggagcgggccttgcagcgctcc-3′; for the p53-CCmutQ60E mutation, 5′-tccgcatgatctacctggagacgttgctg-gccaag-3′ and 5′-cttggccagcaacgtctccaggtagatcatgcgga-3′ primers were used.

For the p53-CCmutE34K-R55E compound mutant, sequential site directed mutagenesis was carried out using the following primers: for the E34K mutation, 5′-gtgggcgacatcga-gcagaagctggagcgctgcaagg-3′ and 5′-ccttgcagcgctccagctt-ctgctcgatgtcgcccac-3′; for the R55E mutation, 5′-aggtgaacca-ggagcgcttcgagatgatctacctgcagacgtt-3′ and 5′-aacgtctgcaggtag-atcatctcgaagcgctcctggttcacct-3′ primers were used.

For the p53-CCmutE46K-R53E compound mutant, sequential site directed mutagenesis was carried out using the following primers: for the E46K mutation, 5′-gcctccattcgg-cgcctgaagcaggaggtgaaccagg-3′ and 5′-cctggttcacctcctgcttcaggcg-ccgaatggaggc-3′; for the R53E mutation, primers 5′-agcag-gaggtgaaccaggagttccgcatgatctacctgca-3′ and 5′-tgcaggta-gatcatgcggaactcctggttcacctcctgct-3′ were used for deletion of R53; primers 5′-gcaggaggtgaaccaggaggagttccgcatgatctacctgc-3′ and 5′-gcaggtagatcatgcggaactcctcctggttcacctcctgc-3′ were used for insertion of 53E.

The plasmids pBIND-p53-CCwt, pBIND-p53CCmutE34K-R55E, pACT-p53-CCwt, and pACT-p53-CCmutE34K-R55E were cloned for the mammalian two-hybrid assay. For pBIND-p53-CCwt and pBIND-p53-CCmutE34K-R55E, DNA encoding p53-CCwt and p53-CCmutE34K-R55E was digested from the pEGFP-p53-CC and pEGFP-p53-CCmutE34K-R55E vectors respectively, using *Bam*HI and *Kpn*I restriction enzymes and subcloned into the pBIND vector (Promega, Madison, WI) at the *Bam*HI and *Kpn*I sites. Similarly, to clone pACT-p53-CCwt and pACT-p53-CCmutE34K-R55E, DNA encoding p53-CCwt and p53-CCmutE34K-R55E was also digested from the pEGFP-p53-CC and pEGFP-p53-CCmutE34K-R55E vectors respectively, using *Bam*HI and *Kpn*I restriction enzymes and subcloned into the pACT vector (Promega) at the *Bam*HI and *Kpn*I sites.

7- AAD Assay. Following manufacturer's instructions and as previously described,[48] T47D, SKOV-3.ip1, and MCF-7 cells were pelleted and resuspended in 500 μL PBS (Invitrogen) containing 1 μM 7-aminoactinomycin D (7-AAD) (Invitrogen) for 30 min prior to analysis by flow cytometry. The assay was performed 48 h after transfection for T47D and MCF-7[49] and 24 h for SKOV-3.ip1. Cells were analyzed and gated for EGFP (with same fluorescence intensity to ensure equal expression of proteins) using the FACSCanto-II (BD-BioSciences, University of Utah Core Facility) and FACSDiva software. Excitation was set at 488 nm and detected at 507 and 660 nm, respectively. Each construct was tested three times ($n = 3$).

Mammalian Two-Hybrid Assay. The pBIND-p53-CCwt (or pBIND-p53-CCmutE34K-R55E) containing the *Renilla reniformis* luciferase gene for normalization, pACT-p53-CCwt (or pACT-p53-CCmutE34K-R55E), and pG5luc (containing firefly luciferase gene, Promega) plasmids were cotransfected using 3.5 μg of each plasmid following the manufacture's recommendations. The pBIND-Id and pACT-MyoD (Promega) plasmids were used for the positive control, and pBIND vector lacking the coiled-coil gene was used as the negative control. Approximately 24 h after transfection, the Dual-Glo Luciferase Assay (Promega) was used to detect both firefly and renilla luminescence as previously.[47] The means from duplicate transfections were taken from three separate experiments ($n = 3$). As per the manufacturer's protocol, a relative response ratio was calculated using the firefly luciferase values normalized to the renilla luciferase values:[50]

$$(\text{sample} - \text{ctrl}^-)/(\text{ctrl}^+ - \text{ctrl}^-)$$

Co-Immunoprecipitation (Co-IP). Co-IP was performed as we have done before.[16] Briefly, T47D cells treated with p53-CCmutE34K-R55e or p53-CCwt were prepared using the Dynabeads Co-Immunoprecipitation Kit (Invitrogen) 24 h post transfection. Approximately 0.2 g of T47D treated cell pellet was lysed in 1.8 mL of extraction buffer B (1 x IP, 100 nM NaCl, 2 mM $MgCl_2$, 1 mM DTT, 1% protease inhibitor). The lysate was incubated for 30 min at 4 °C with 1.5 mg of Dynabeads coupled with anti-GFP antibody (ab290, Abcam). Immune complexes were then collected on a magnet, washed, and eluted using 60 μL of elution buffer. Finally, the eluted complexes were denatured and Western blots were carried out as described before.[16] The coiled-coil domain was probed using anti-Bcr (sc-885, Santa Cruz Biotechnology, Santa Cruz, CA). The primary antibody was detected with antirabbit HRP-conjugated antibody (#7074S, Cell Signaling Technology, Danvers, MA) before the addition of SuperSignal West Pico chemiluminescent substrate (Thermo Scientific, Waltham, MA). Signals were detected using a FluorChem FC2 imager and software (Alpha Innotech, Santa Clara, CA). Each co-IP was repeated at least three times. A semiquantitative densitometry analysis was carried out by normalizing the detected Bcr band to either p53-CCwt or p53-CCmutE34K-R55E as described before.[51]

Statistical Analysis. For in vitro experiments, one-way ANOVA with Bonferroni's post hoc test was used to compare the different groups and controls. A value of $p < 0.05$ was considered statistically significant. Error bars represent standard deviations from at least three independent experiments ($n = 3$).

RESULTS

In silico modeling of coiled-coil structures and estimation of binding free energies. Computational modeling and atomistic biomolecular simulations were employed to facilitate the design of coiled-coil mutations which serve to enhance homo-oligomerization of the modified coils while disrupting hetero-oligomerization with the native coiled-coil region of Bcr. Initial simulations estimated differences in relative binding free energy of the modified coils to predict the most effective coiled-coil design (Table 2). All four mutants from Table 1 were rationally designed based on optimization of the electrostatic interactions and the potential

Table 2. Energetic analysis of p53-CC wild-type and mutants coiled-coil dimers as obtained by MM-PBSA

Mutations	$\Delta G_{binding}$	S.E.
None (CCwt)	kcal/mol	
Homodimer	-59.5	0.8
p53-CCmutE34K-R55E		
Homodimer	-51.9	0.8
Heterodimer	-37.5	0.8
p53-CCmutE46K-R53E		
Homodimer	-58.2	0.7
Heterodimer	-51.0	0.7
p53-CCmutS41R		
Homodimer	-80.0	0.8
Heterodimer	-54.8	0.8
p53-CCmutQ60E		
Homodimer	-76.6	0.7
Heterodimer	-59.6	0.7

for salt bridge formation identified in the helical wheel structure of the CC motif (helical wheel characterized previously by Taylor et al.).[27] The designed mutations aimed to enhance homo-oligomerization by either enhancement of the binding interaction between modified coiled-coils (CCmutS41R and CCmutQ60E), or disruption of the interaction between mutant and wild-type coiled-coils (CCmutE34K-R55E and CCmutE46K-R53E). Production molecular dynamics were carried out on a total of nine independent simulations, in which trajectories were generated for each of the modified coils paired with either itself (homodimer) or CCwt (heterodimer). A wild-type coiled-coil homodimer was used as a control.

An MM-PBSA postprocessing energetic analysis of the MD trajectories of the dimers[45,46] was performed on each independent simulation to identify the optimal modifications to enhance self-oligomerization (see Table 2). Modified coiled-coils, which were designed to promote self-oligomerization by increasing the binding stability (p53-CCmutS41R and p53-CCmutQ60E), had relatively strong binding for their homodimers (Table 2, ΔG= −80.0 kcal/mol and ΔG= −76.6 kcal/mol, respectively). However, they failed to disrupt binding to the native CCwt (Table 2, ΔG= −54.8 kcal/mol and ΔG= −59.6 kcal/mol, respectively), suggesting that creating additional salt bridges *will not* prevent p53-CC from binding to endogenous Bcr. Results (Table 2) suggest that the best approach to increase self-oligomerization among the modified coiled-coils while minimizing hetero-oligomerization with Bcr is to increase the binding specificity of the coiled-coil for itself through the reversing of existing salt bridges (resembled by CCmutE34K-R55E and CCmutE46K-R53E). Energetic analyses of the modified coiled-coils featuring a reversal of salt bridges (p53-CCmutE34K-R55E and p53-CCmutE46K-R53E) revealed minimal destabilization of the homodimers p53-CCmutE34K-R55E and p53-CCmutE46K-R53E (Table 2, ΔG= −51.9 kcal/mol and ΔG= −58.2 kcal/mol, respectively), and in the case of the p53-CCmutE34K-R55E mutant, a significant destabilization of the heterodimer with CCwt (Table 2, ΔG= −37.5 kcal/mol). The p53-CCmutE46K-R53E mutant heterodimer with CCwt was minimally destabilized (ΔG= −51.0 kcal/mol). Therefore, of the four rationally designed mutants, p53-CCmutE34K-R55E is the only variant which displays both of the desired characteristics of homodimer stabilization and disruption of CCwt binding, suggesting that the CCmutE34K-R55E mutant provides the most effective strategy to promote self-oligomerization and prevent interaction with native Bcr.

Results were obtained using the MM-PBSA functionality of the AmberTools suite of programs.[36] Every 20 ns of simulation time, energetic analyses were performed on 5 ns snapshots of simulation (0−5 ns, 20−25 ns, 40−45 ns, etc.) at 25 ps intervals to examine the evolution of relative free binding energies of each system over time. The results reflect the lowest calculated free energies of the nine different MD trajectories (See Supporting Information 1 for more information).

Initial screening for in vitro activity. Next, we carried out initial in vitro screening of the activity of each p53-CCmut to examine if our proposed mutations abrogate the tumor suppressor function of p53-CC. Active p53-CC has been shown previously to induce significant levels of cell death in T47D breast cancer cells.[16] Hence, the 7-AAD assay, which stains apoptotic and necrotic cells,[52,53] served as a screening tool to measure tumor suppressor function of the different p53-CC mutants (Figure 2). Surprisingly, all of the designed mutations

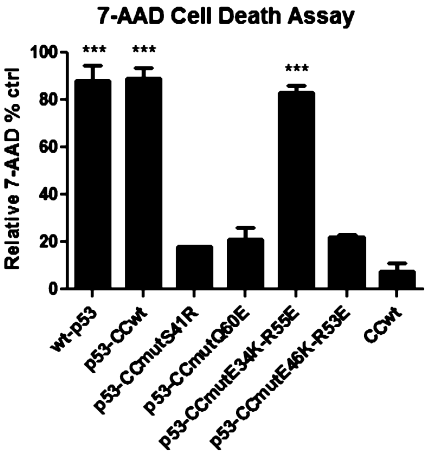

Figure 2. Tumor suppressor activity screening using the 7-AAD assay was conducted in T47D cells 48 h post transfection. p53-CCmutE34K-R55E is the only candidate that retains the ability to induce cell death in a similar to p53-CCwt and the wt-p53 control. CCwt was used as a negative control. Statistical analysis was performed using one-way ANOVA with Bonferroni's post hoc test; *** $p < 0.001$ compared to CCwt negative control. Error bars represent standard deviations (n = 3).

led to abolishment of p53-CC function, except for the CCmutE34K-R55E compound mutation. Figure 2 illustrates that p53-CCmutE34K-R55E (fifth bar) retains the apoptotic activity of p53-CCwt and wt-p53 (first two bars). As expected, the negative control CCwt alone shows no apoptotic activity in the 7-AAD assay (last bar). These findings suggest that the S41R, Q60E, and E46K-R53E mutations may disrupt the oligomerization of CC, lead to instability of the coiled-coil domain, or alter the conformation of p53, resulting in loss of tumor suppressor function (third, fourth and sixth bars, respectively).

Although computational design and modeling implies that S41R, Q60E, and E46K-R53E may be candidates for increasing salt bridge formation and binding stability, the data in Figure 2 illustrates that introducing any of these mutations on the CC domain leads to biological inactivation of the chimeric p53-CC. Therefore, we narrowed down our mutant candidate to p53-CCmutE34K-R55E, which favors homo-oligomer formation

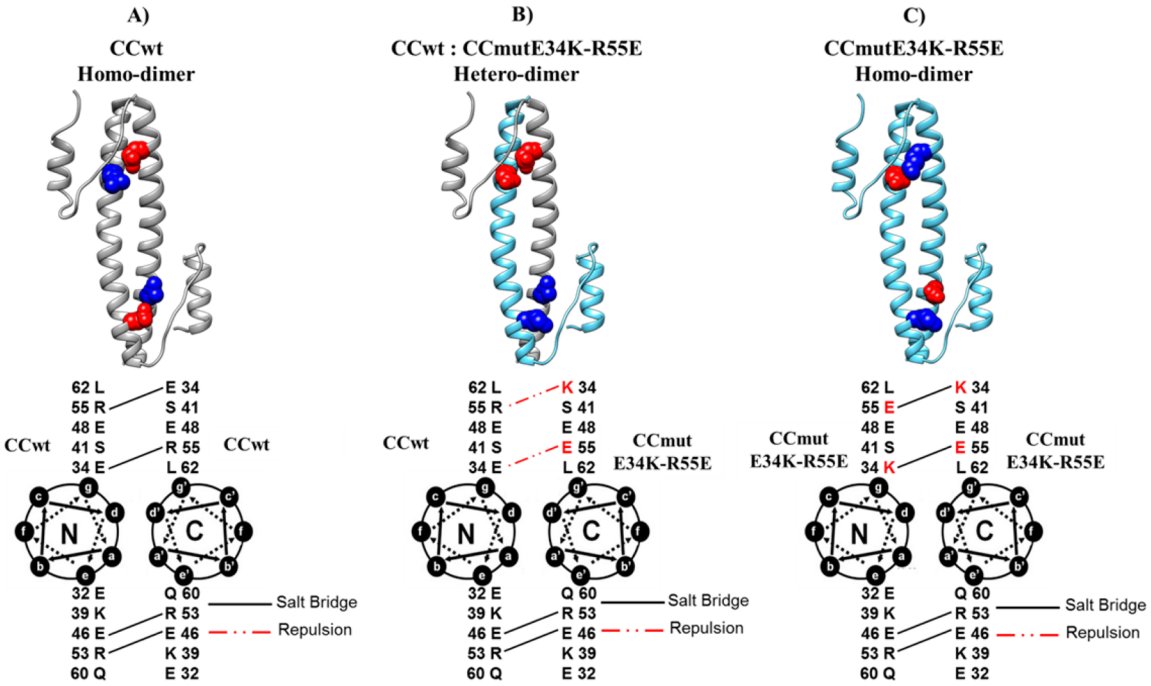

Figure 3. Ribbon diagrams with corresponding helical wheels of CCwt homodimer (A), CCwt-CCmutE34K-R55E heterodimer (B), and CCmutE34K-R55E homodimer (C). Gray ribbons represent the CCwt domain, and cyan ribbons represent the CCmutE34K-R55E domain. The side chains of key residues (Glu/Lys-34 and Arg/Glu-55) are shown as red (acidic) or blue (basic). Solid lines indicate salt bridges, while the long dash double dotted line represents charge−charge repulsions.

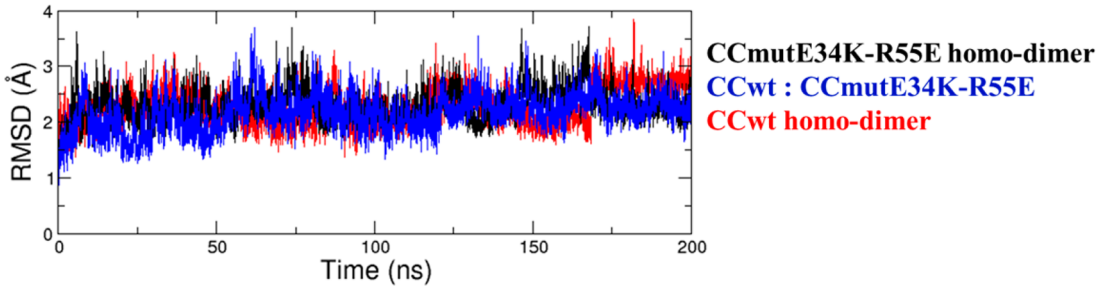

Figure 4. Time course of the deviation of the MD structures of the Bcr coiled-coil region (CCwt) and CCmut E34K-R55E to the experimental reference structure. One dimensional RMSD analyses was performed to monitor the structural variance of the mutant CCmutE34K-R55E homodimer (black) and the CCwt:CCmutE34K-R55E (blue) relative to the CCwt homodimer (red). Results suggest the modified coiled-coil homodimer remains close to the reference experimental structure throughout the 200 ns trajectory.

over heterodimerization with CCwt of Bcr (Table 2), while retaining the biological activity of p53-CCwt (Figure 2). Figure 3 shows ribbon diagrams with corresponding helical wheels (below) of CCwt homodimer (Figure 3A), CCwt:CCmutE34K-R55E heterodimer (Figure 3B), and CCmutE34K-R55E homodimer (Figure 3C). As expected from our computational design, the compound mutant CCmutE34K-R55E does not lead to formation of new additional ionic interactions (salt bridges). Instead, the same two salt bridges found in the CCwt:CCwt homodimer (Figure 3A) are preserved (but reversed) in the CCmutE34K-R55E:CCmutE34K-R55E homodimer (Figure 3C). However, Figure 3B illustrates that two possible charge−charge repulsions in the CCwt:CCmutE34K-R55E heterodimer could form, which have the potential to reduce p53-CCmutE34K-R55E interaction with Bcr (aka CCwt).

Global stability of p53-CCmutE34K-R55E. Several analyses were performed to evaluate the stability of CCmutE34K-R55E homodimer relative to the CCwt homodimer and the CCwt:CCmutE34K-R55E heterodimer. RMSD analyses of the MD sampled structures to the initial structures revealed that both the mutant homodimer and mutant heterodimers remained close to their initial structures, as was observed with the CCwt homodimer (Figure 4). The atomic positional fluctuations (Supporting Information 2) of C_α backbone atoms were recorded to identify regions of flexibility in response to the induced mutations, revealing an increase in flexibility of the CCmutE34K-R55E mutant when paired to CCwt, in the region of the E34K-R55E mutations. This can be attributed to the destabilization of the coiled-coils by the unfavorable electrostatic interactions occurring between the mutant and wild-type coiled-coils. A slight increase in the flexibility of the CCmutE34K-R55E homodimer is observed at N-termini and C-termini α-helical regions (Residues 1−10 and 124−134, respectively); however a DSSP secondary structure analysis[44] revealed no loss in coiled-coil helicity in the CCmutE34K-R55E homodimer relative to the CCwt homodimer (Table 3, helicity= 71.8% and 71.6%, respectively),

dx.doi.org/10.1021/mp500202p | Mol. Pharmaceutics 2014, 11, 2442−2452

Table 3. Relative Helicity of the Modified Coiled-Coil Region CCmutE34K-R55E Relative to the Native Coiled-Coil from Bcr (CCwt)

	secondary structure		hydrogen bonds	
mutations	helicity (%)	S.D. (%)	*i*, *i* + 4 hydrogen bonding (%)	S.D. (%)
none (CCwt)				
homodimer	71.6	9.6	32.1	3.7
CCmutE34K-R55E				
homodimer	71.8	10.6	31.3	3.6
heterodimer	71.1	11.5	31.3	3.7

suggesting that the α-helical dimerization interface remains stable. Analysis of α-helical specific hydrogen bonding interactions (between backbone atoms of i and i + 4 residues) revealed no significant difference in hydrogen bonding patterns between the CCmutE34K-R55E and CCwt homodimers (Table 3; i and i + 4 hydrogen bond = 33.1% and 32.1%, respectively) to indicate a loss of coiled-coil stability due to the observed atomic positional fluctuations. Together, these results suggest that the compound mutation E34K-R55E does not affect the stability of the coiled-coil, supporting the existing evidence (Figure 2) that p53-CCmutE34K-R55E forms biologically active oligomers, retaining transcriptional and tumor suppressor activity of p53.

A DSSP secondary structure analysis was performed on each of the nine MD trajectories, characterizing the phi (ϕ) and psi (ψ) backbone dihedral torsions of each residue to calculate the percentage of coiled-coil residues defined as α-helical. The percentage of interhelical hydrogen bonds between i and i + 4 residues (specific to α helices) formed throughout the trajectory was compared to the total number of potential i, i + 4 hydrogen bonding interactions (total number of residues in each coiled-coil minus four).

Binding Assay Validates Design. To specifically address whether our lead mutant compound CCmutE34K-R55E limited hetero-oligomerization with CCwt (found in endogenous Bcr), the mammalian two-hybrid binding assay[50] was carried out. Figure 5 demonstrates that formation of CCmutE34K-R55E homo-oligomers (third bar) is more favored than CCwt:CCmutE34K-R55E hetero-oligomerization (middle bar). Although CCmutE34K-R55E homodimerization leads to preserving all four possible salt bridges that normally exist in the CCwt homodimer (see Figure 3C vs A), CCmutE34K-R55E heterodimerization with CCwt may produce two new possible charge−charge repulsions (see Figure 3B). In addition, Figure 5 shows no significant difference in the binding between CCwt and CCmutE34K-R55E homodimers (first and third bars), as expected. This similarity in binding between CCwt vs CCmutE34K-R55E homodimers converges with the data obtained from our computational modeling of binding energies (Table 2; also illustrated in Figure 3), in which no change of the total number of salt bridges occur as a consequence of introducing the E34K-R55E mutation to the coiled-coil domain.

p53-CCmutE34K-R55E Interaction with Endogenous Bcr. The mammalian two-hybrid assay illustrates the ability of our CCmutE34K-R55E compound mutation in limiting the interaction of p53-CCmutE34K-R55E with the CCwt domain of endogenous Bcr in cells. To substantiate the mammalian two-hybrid assay data, a coimmunoprecipitation assay was performed to determine if exogenously added p53-CCmutE34K-R55E has limited interaction with the CCwt domain of endogenous Bcr compared to p53-CCwt. Cell lysates transfected with either p53-CCmutE34K-R55E or p53-CCwt were immunoprecipitated as we have done before.[16] Endogenous Bcr that could potentially coimmunoprecipitate was probed using anti-CCwt antibody. Figure 6A shows that endogenous Bcr coimmunoprecipitates (i.e., interacts) with p53-CCmutE34K-R55E to a lesser extent compared to p53-CCwt. Furthermore, we carried out Bcr mean band densitometry analyses from three separate coimmunoprecipitation assays. Figure 6B shows that p53-CCwt hetero-oligomerization with endogenous Bcr is 2-fold higher than the p53-CCmutE34K-R55E interaction with Bcr. These findings indicate that the E34K-R55E compound mutation reduces hetero-oligomerization with endogenous Bcr compared to CCwt interaction with Bcr, presumably due to the formation of charge−charge repulsions (see Figure 3B). It should be noted that prominent double secondary bands are detected by this anti-CCwt antibody even in untreated cell lysates (data not shown).

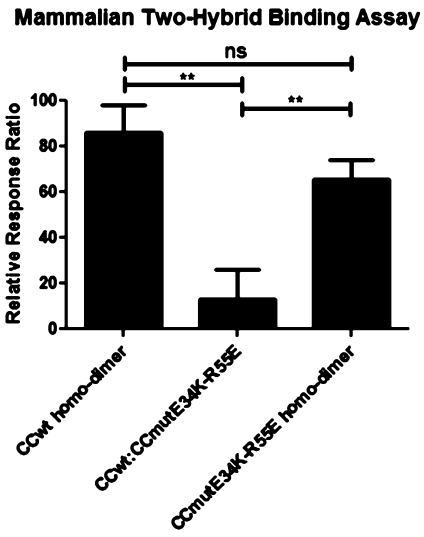

Figure 5. Binding of CCmutE34K-R55E homo- and heterodimers with CCwt tested using the mammalian-two hybrid assay. The assay was carried out in COS-7 cells 24 h post transfection. Both CCwt and CCmutE34K-R55E have similar binding as indicated by the first and third bar, respectively. The mammalian-two hybrid assay revealed weak binding of CCmutE34K-R55E heterodimerization with CCwt. Statistical analysis was performed using one-way ANOVA with Bonferroni's post hoc test. ** $p < 0.01$, ns = not significant. Error bars represent standard deviations (n = 3).

p53-CCmutE34K-R55E Induces Apoptosis Regardless of the p53 Status or Cancer Cell Type. To ensure that the ability of p53-CCmutE34K-R55E to induce cell death is neither dependent on endogenous p53 status nor cancer cell line specific, its apoptotic activity was tested in three different cancer cell lines: SKOV-3.ip1 human ovarian cancer cells (p53-null),[54] MCF-7 human breast cancer cells (wild-type but mislocalized p53),[55] and T47D human breast carcinoma cells (mutant p53).[56] Figure 7A−C demonstrates that p53-CCmutE34K-R55E is capable of inducing cell death similarly to p53-CCwt and wt-p53, regardless of the endogenous p53 status or cancer cell line.

DISCUSSION

Because domain swapping to create p53-CC could result in p53-CC interacting with endogenous Bcr, we mutated p53-CC

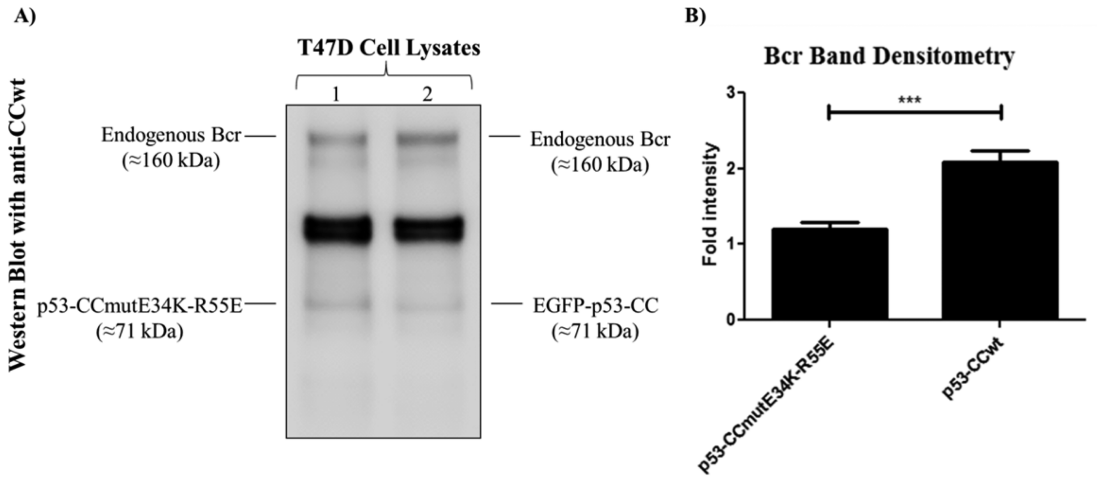

Figure 6. Interaction of p53-CCmutE34K-R55E and p53-CC with endogenous Bcr was investigated in T47D cells via co-IP. (A) A representative cropped Western blot of protein complexes coimmunoprecipitated using anti-GFP antibody is shown. Left lane, endogenous Bcr (160 kDa) coimmunoprecipitates with p53-CCmutE34K-R55E (71 kDa) to a lesser extent compared to that with p53-CC (71 kDa) in the right lane. (B) Semiquantitative densitometric analyses was carried out as described before[51] to evaluate Bcr interaction with p53-CCmutE34K-R55E and p53-CC and represented as Bcr band density as fold intensity of the expression level of corresponding construct (p53-CCmutE34K-R55E and p53-CC) in each sample. Mean values were analyzed using one-way ANOVA with Bonferroni's post hoc test. *** $p < 0.001$. Error bars represent standard deviations ($n = 3$).

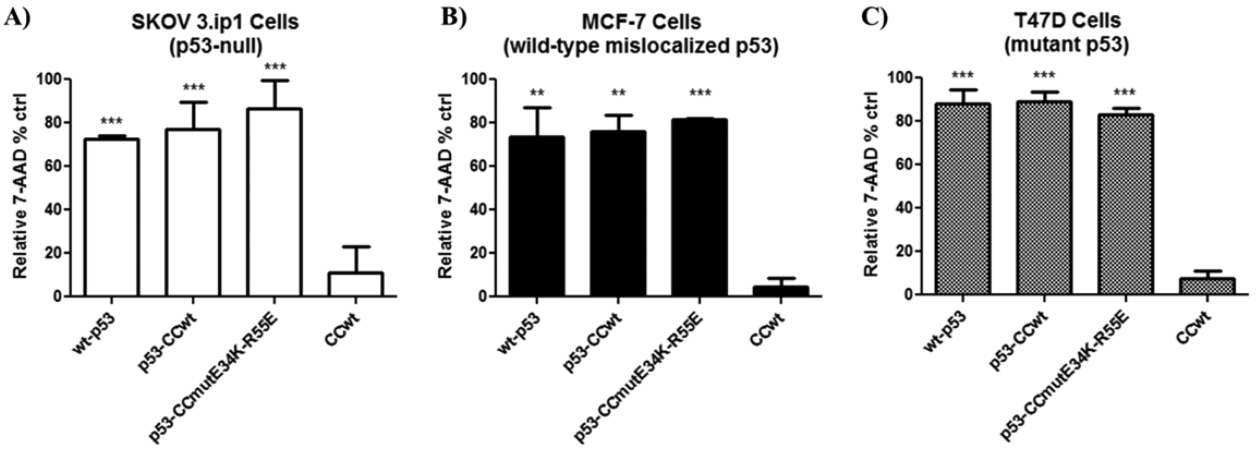

Figure 7. 7-AAD assay was conducted in three different cell lines with varying p53 status (A) SKOV 3.ip1, (B) MCF-7, and (C) T47D cells. In all three cases, p53-CCmutE34K-R55E was capable of inducing cell death in a similar fashion compared to p53-CC and wt-p53, regardless of the endogenous p53 status or the cancer cell line used. Statistical analysis was performed using one-way ANOVA with Bonferroni's post hoc test. ** $p < 0.01$ and *** $p < 0.001$.

to avoid this. The implications of possible binding of endogenous Bcr are unknown, but may be undesired, as Bcr is a ubiquitous protein involved in inflammatory pathways and cell proliferation.[21] Because no other proteins in cells contain the Bcr CCwt motif, the sequence-specific interaction with Bcr CCwt is the only one we need be concerned with eliminating.

In this report, we designed mutations in our alternative oligomerization domain, the coiled-coil, to avoid interaction with Bcr. Computationally designed and modeled mutations in the CC domain[47] were developed to minimize interactions with native endogenous Bcr. On the basis of the initial examination of the CC motif, several possible mutation sites were identified and summarized in Table 1 with the rationale behind designing each mutation. In addition, Figure 1 shows helical diagrams representing the CCwt, the modified CC domain (CCmut), and the hypothesized changes in electrostatic interactions (salt bridges). Two different modified coiled-coils with a single point mutation each were designed to enhance self-oligomerization. Residues Ser-41 and Gln-60 are arranged opposite of charged residues Glu-48 and Lys-39, such that the mutations S41R and Q60E serve to create additional salt bridges in the coiled-coil dimers. In the first mutant, Ser-41 was mutated to Arg, creating two new salt bridges via interaction with Glu-48 (Figure 1B). In the second mutant, Gln-60 was mutated to Glu, creating two new salt bridges via interaction with Lys-39 (Figure 1C).

Furthermore, two different modified coiled-coils with two point mutations each (compound mutants) were designed to increase binding specificity of the modified coiled-coil for itself by disrupting affinity for CCwt. By reversing the charge of existing salt bridges (dashed line highlighted in green in Figure 1 D and E), a scenario is created in which charge repulsion disrupts the binding of the CCwt to the modified coiled-coils. In the p53-CCmutE34K-R55E mutant, the salt bridge between Glu-34 and Arg-55 is effectively reversed by introducing the mutations E34K and R55E. Similarly, the p53-CCmutE46K-

dx.doi.org/10.1021/mp500202p | Mol. Pharmaceutics 2014, 11, 2442−2452

R53E mutant features the mutations E46K and R53E to reverse the salt bridge between Glu-46 and Arg-53.

Molecular modeling, MD simulation, and free energy analysis revealed the ranking of our different modifications in terms of minimizing CCwt-CCmut hetero-oligomerization (Table 2). On one hand, free binding energy analysis by MM-PBSA revealed that CCmutS41R and CCmutQ60E may both have relatively strong homo-oligomer binding stability (Table 2, ΔG = −80.0 kcal/mol and ΔG = −76.6 kcal/mol, respectively). However, the same analysis revealed that both, CCmutS41R and CCmutQ60E, also have similar or increased binding stability for their heterodimers with CCwt (Table 2, ΔG = −54.8 kcal/mol and ΔG = −59.6 kcal/mol, respectively). In addition, there is no significant difference in binding energies between CCmutE46K-R53E homodimers and heterodimers (Table 2, ΔG = −58.2 kcal/mol and ΔG = −51.0 kcal/mol, respectively). On the other hand, free binding energy analysis showed that CCmutE34K-R55E may be a suitable candidate for minimizing interactions with CCwt, with CCmutE34K-R55E disfavoring interaction with CCwt. A significant difference in the binding free energies exist between the CCmutE34-R55E homodimer and heterodimer with CCwt (Table 2, ΔG = −51.9 kcal/mol and ΔG = −37.5 kcal/mol, respectively). This result suggests that CCmutE34K-R55E favors homo-oligomerization over hetero-oligomerization with CCwt of Bcr. Furthermore, the free binding energy for CCmutE34K-R55E heterodimer with CCwt is less favored (Table 2, ΔG = −37.5 kcal/mol) compared to that of CCwt homo-oligomer (Table 2, ΔG = −51.9 kcal/mol). To test if our possible mutations led to any abrogation in p53-CC activity, we carried out an in vitro cell death assay in which p53-CC has been proven previously to induce cell death (in T47D cells).[16] Figure 2 showed that all mutants (p53-CCmutS41R, p53-CCmutQ60E, and p53-CCmutE46K-R53E) have lost the tumor suppressor activity of p53-CC except for the compound mutant p53-CCmutE34K-R55E. Thus, p53-CCmutE34K-R55E was the lead, eliminating the need to test the inactive mutants in the remaining experiments.

Both the mammalian two-hybrid assay (Figure 5) and the coimmunoprecipitation experiment (Figure 6) validate the computational modeling and strongly indicate that p53-CCmutE34K-R55E minimizes the interaction with CCwt of endogenous Bcr in cells, suggesting that our hypothesized interactions are indeed occurring. Finally, we confirmed that the tumor suppressor activity (measured by apoptotic activity) of p53-CCmutE34K-R55E remains consistent regardless of endogenous p53 status or the type of cancer cell line as shown in Figure 7.

This study showed how in silico modeling can guide experimental design (as we have done before)[57] and that further iterations of in vitro design resulted in an enhanced version of our chimeric p53.[16] The resulting rationally designed p53-CCmutE34K-R55E avoids binding to endogenous Bcr and yet retains potent apoptotic activity in a variety of cancer cell lines, regardless of p53 status. This construct will be used for future gene therapy experiments for treatment of cancers characterized by p53 dysfunction, which represent over half of all human cancers.

■ ASSOCIATED CONTENT

Supporting Information

MM-PBSA energetic analysis and atomic positional fluctuations. This material is available free of charge via the Internet at http://pubs.acs.org.

■ AUTHOR INFORMATION

Corresponding Author

*E-mail: carol.lim@pharm.utah.edu. Phone: 1-801-587-9711. Fax: 1-801-585-3614. Address: 30 S. 2000 E. Rm. 2916, Salt Lake City, Utah 84112, United States.

Author Contributions

The manuscript was written through contributions of all authors. All authors have given approval to the final version of the manuscript.

Notes

The authors declare no competing financial interest.

■ ACKNOWLEDGMENTS

We would like to thank Jennifer Gläsel, Mohanad Mossalam, Ben Bruno, and Geoff Miller for scientific discussions. Research reported in this publication was supported by the National Cancer Institute of the National Institutes of Health under award number R01-CA151847. The authors acknowledge the use of DNA/Peptide Core and Flow Cytometry Core (NCI Cancer Center Support Grant P30 CA042014, Huntsman Cancer Institute). We also acknowledge support of funds in conjunction with grant P30 CA042014 awarded to Huntsman Cancer Institute.

■ ABBREVIATIONS

wt-p53, wild-type p53; TD, tetramerization domain; CC, coiled-coil; Bcr, breakpoint cluster region; CML, chronic myeloid leukemia; CCwt, wild-type coiled-coil

■ REFERENCES

(1) Staples, O. D.; Steele, R. J. C.; Lain, S. p53 as a therapeutic target. *Surgeon* **2008**, *6* (4), 240−243.

(2) Abrahamson, J. L.; Lee, J. M.; Bernstein, A. Regulation of p53-mediated apoptosis and cell cycle arrest by Steel factor. *Mol. Cell. Biol.* **1995**, *15* (12), 6953−60.

(3) Wagner, A. J.; Kokontis, J. M.; Hay, N. Myc-mediated apoptosis requires wild-type p53 in a manner independent of cell cycle arrest and the ability of p53 to induce p21waf1/cip1. *Genes Dev.* **1994**, *8* (23), 2817−30.

(4) Levine, A. J.; Oren, M. The first 30 years of p53: growing ever more complex. *Nat. Rev. Cancer* **2009**, *9* (10), 749−58.

(5) Hollstein, M.; Sidransky, D.; Vogelstein, B.; Harris, C. C. p53 mutations in human cancers. *Science* **1991**, *253* (5015), 49−53.

(6) Olivier, M.; Hollstein, M.; Hainaut, P. TP53 mutations in human cancers: origins, consequences, and clinical use. *Cold Spring Harbor Perspect. Biol.* **2010**, *2* (1), a001008.

(7) El-Aneed, A. An overview of current delivery systems in cancer gene therapy. *J. Controlled Release* **2004**, *94* (1), 1−14.

(8) Lang, F. F.; Bruner, J. M.; Fuller, G. N.; Aldape, K.; Prados, M. D.; Chang, S.; Berger, M. S.; McDermott, M. W.; Kunwar, S. M.; Junck, L. R.; Chandler, W.; Zwiebel, J. A.; Kaplan, R. S.; Yung, W. K. A. Phase I Trial of Adenovirus-Mediated p53 Gene Therapy for Recurrent Glioma: Biological and Clinical Results. *J. Clin. Oncol.* **2003**, *21* (13), 2508−2518.

(9) BLAGOSKLONNY, M. V. p53 from complexity to simplicity: mutant p53 stabilization, gain-of-function, and dominant-negative effect. *FASEB J.* **2000**, *14* (13), 1901−1907.

(10) Turner, N.; Moretti, E.; Siclari, O.; Migliaccio, I.; Santarpia, L.; D'Incalci, M.; Piccolo, S.; Veronesi, A.; Zambelli, A.; Del Sal, G.; Di Leo, A. Targeting triple negative breast cancer: Is p53 the answer? *Cancer Treat. Rev.* **2013**, *39* (5), 541−50.
(11) Waterman, M. J.; Waterman, J. L.; Halazonetis, T. D. An engineered four-stranded coiled coil substitutes for the tetramerization domain of wild-type p53 and alleviates transdominant inhibition by tumor-derived p53 mutants. *Cancer Res.* **1996**, *56* (1), 158−63.
(12) Willis, A.; Jung, E. J.; Wakefield, T.; Chen, X. Mutant p53 exerts a dominant negative effect by preventing wild-type p53 from binding to the promoter of its target genes. *Oncogene* **2004**, *23* (13), 2330−8.
(13) Kern, S.; Kinzler, K.; Bruskin, A.; Jarosz, D.; Friedman, P.; Prives, C.; Vogelstein, B. Identification of p53 as a sequence-specific DNA-binding protein. *Science* **1991**, *252* (5013), 1708−1711.
(14) Milner, J.; Medcalf, E. A. Cotranslation of activated mutant p53 with wild type drives the wild-type p53 protein into the mutant conformation. *Cell* **1991**, *65* (5), 765−74.
(15) Srivastava, S.; Wang, S.; Tong, Y. A.; Hao, Z. M.; Chang, E. H. Dominant negative effect of a germ-line mutant p53: a step fostering tumorigenesis. *Cancer Res.* **1993**, *53* (19), 4452−5.
(16) Okal, A.; Mossalam, M.; Matissek, K. J.; Dixon, A. S.; Moos, P. J.; Lim, C. S. A Chimeric p53 Evades Mutant p53 Transdominant Inhibition in Cancer Cells. *Mol. Pharm.* **2013**, *10* (10), 3922−33.
(17) Jeffrey, P.; Gorina, S.; Pavletich, N. Crystal structure of the tetramerization domain of the p53 tumor suppressor at 1.7 angstroms. *Science* **1995**, *267* (5203), 1498−1502.
(18) Zhao, X.; Ghaffari, S.; Lodish, H.; Malashkevich, V. N.; Kim, P. S. Structure of the Bcr-Abl oncoprotein oligomerization domain. *Nat. Struct. Biol.* **2002**, *9* (2), 117−20.
(19) Deininger, M. W.; Goldman, J. M.; Melo, J. V. The molecular biology of chronic myeloid leukemia. *Blood* **2000**, *96* (10), 3343−56.
(20) Woessner, D. W.; Lim, C. S.; Deininger, M. W. Development of an effective therapy for chronic myelogenous leukemia. *Cancer J.* **2011**, *17* (6), 477−86.
(21) Alexis, J. D.; Wang, N.; Che, W.; Lerner-Marmarosh, N.; Sahni, A.; Korshunov, V. A.; Zou, Y.; Ding, B.; Yan, C.; Berk, B. C.; Abe, J. Bcr kinase activation by angiotensin II inhibits peroxisome-proliferator-activated receptor gamma transcriptional activity in vascular smooth muscle cells. *Circ. Res.* **2009**, *104* (1), 69−78.
(22) Yi, S. J.; Groffen, J.; Heisterkamp, N. Bcr is a substrate for Transglutaminase 2 cross-linking activity. *BMC Biochem.* **2011**, *12*, 8.
(23) Alexis, J. D.; Wang, N.; Che, W.; Lerner-Marmarosh, N.; Sahni, A.; Korshunov, V. A.; Zou, Y.; Ding, B.; Yan, C.; Berk, B. C.; Abe, J. Bcr kinase activation by angiotensin II inhibits peroxisome-proliferator-activated receptor gamma transcriptional activity in vascular smooth muscle cells. *Circ. Res.* **2009**, *104* (1), 69−78.
(24) Mason, J. M.; Arndt, K. M. Coiled coil domains: stability, specificity, and biological implications. *ChemBioChem* **2004**, *5* (2), 170−6.
(25) Lupas, A. Coiled coils: new structures and new functions. *Trends Biochem. Sci.* **1996**, *21* (10), 375−382.
(26) Burkhard, P.; Stetefeld, J.; Strelkov, S. V. Coiled coils: a highly versatile protein folding motif. *Trends Cell Biol.* **2001**, *11* (2), 82−88.
(27) Taylor, C. M.; Keating, A. E. Orientation and oligomerization specificity of the Bcr coiled-coil oligomerization domain. *Biochemistry* **2005**, *44* (49), 16246−56.
(28) McWhirter, J. R.; Galasso, D. L.; Wang, J. Y. A coiled-coil oligomerization domain of Bcr is essential for the transforming function of Bcr-Abl oncoproteins. *Mol. Cell. Biol.* **1993**, *13* (12), 7587−7595.
(29) Pettersen, E. F.; Goddard, T. D.; Huang, C. C.; Couch, G. S.; Greenblatt, D. M.; Meng, E. C.; Ferrin, T. E. UCSF Chimera–a visualization system for exploratory research and analysis. *J. Comput. Chem.* **2004**, *25* (13), 1605−12.
(30) Shapovalov, M. V.; Dunbrack, R. L., Jr. A smoothed backbone-dependent rotamer library for proteins derived from adaptive kernel density estimates and regressions. *Structure* **2011**, *19* (6), 844−58.
(31) Hornak, V.; Abel, R.; Okur, A.; Strockbine, B.; Roitberg, A.; Simmerling, C. Comparison of multiple Amber force fields and development of improved protein backbone parameters. *Proteins* **2006**, *65* (3), 712−25.
(32) Cornell, W. D.; Cieplak, P.; Bayly, C. I.; Gould, I. R.; Merz, K. M.; Ferguson, D. M.; Spellmeyer, D. C.; Fox, T.; Caldwell, J. W.; Kollman, P. A. A Second Generation Force Field for the Simulation of Proteins, Nucleic Acids, and Organic Molecules. *J. Am. Chem. Soc.* **1995**, *117* (19), 5179−5197.
(33) Jorgensen, W. L.; Chandrasekhar, J.; Madura, J. D.; Impey, R. W.; Klein, M. L. Comparison of simple potential functions for simulating liquid water. *J. Chem. Phys.* **1983**, *79* (2), 926−935.
(34) Joung, I. S.; Cheatham, T. E., III Determination of alkali and halide monovalent ion parameters for use in explicitly solvated biomolecular simulations. *J. Phys. Chem. B* **2008**, *112* (30), 9020−41.
(35) Berendsen, H. J. C.; Postma, J. P. M.; van Gunsteren, W. F.; DiNola, A.; Haak, J. R. Molecular dynamics with coupling to an external bath. *J. Chem. Phys.* **1984**, *81* (8), 3684−3690.
(36) Case, D. A.; Darden, T., Cheatham, T. E., III; Simmerling, C. L.; Wang, J.; Duke, R. E.; Luo, R.; Walker, R. C.; Zhang, W.; Merz, K. M.; Roberts, B.; Hayik, S.; Roitberg, A.; Seabra, G.; Swails, J.; Goetz, A.W.; I. Kolossváry, Wong, K. F.; Paesani, F.; Vanicek, J.; Wolf, R. M.; Liu, J.; Wu, X.; Brozell, S. R.; Steinbrecher, T.; Gohlke, H.; Cai, Q.; Ye, X.; Wang, J.; Hsieh, M.-J.; Cui, G.; Roe, D. R.; Mathews, D. H.; Seetin, M. G.; R. Salomon-Ferrer, Sagui, C.; Babin, V.; Luchko, T.; Gusarov, S.; Kovalenko, A.; Kollman, P. A. *AMBER 12*; University of California: San Francisco, CA, 2012.
(37) Pearlman, D. A.; Case, D. A.; Caldwell, J. W.; Ross, W. S.; Cheatham Iii, T. E.; DeBolt, S.; Ferguson, D.; Seibel, G.; Kollman, P. AMBER, a package of computer programs for applying molecular mechanics, normal mode analysis, molecular dynamics and free energy calculations to simulate the structural and energetic properties of molecules. *Comput. Phys. Commun.* **1995**, *91* (1−3), 1−41.
(38) Zwanzig, R. Nonlinear generalized Langevin equations. *J. Stat. Phys.* **1973**, *9* (3), 215−220.
(39) Loncharich, R. J.; Brooks, B. R.; Pastor, R. W. Langevin dynamics of peptides: the frictional dependence of isomerization rates of N-acetylalanyl-N′-methylamide. *Biopolymers* **1992**, *32* (5), 523−35.
(40) Essmann, U.; Perera, L.; Berkowitz, M. L.; Darden, T.; Lee, H.; Pedersen, L. G. A smooth particle mesh Ewald method. *J. Chem. Phys.* **1995**, *103* (19), 8577−8593.
(41) Ryckaert, J.-P.; Ciccotti, G.; Berendsen, H. J. C. Numerical integration of the cartesian equations of motion of a system with constraints: molecular dynamics of n-alkanes. *J. Comput. Phys.* **1977**, *23* (3), 327−341.
(42) Roe, D. R.; Cheatham, T. E. PTRAJ and CPPTRAJ: Software for Processing and Analysis of Molecular Dynamics Trajectory Data. *J. Chem. Theory Comput.* **2013**, *9* (7), 3084−3095.
(43) Shao, J.; Tanner, S. W.; Thompson, N.; Cheatham, T. E. Clustering Molecular Dynamics Trajectories: 1. Characterizing the Performance of Different Clustering Algorithms. *J. Chem. Theory Comput.* **2007**, *3* (6), 2312−2334.
(44) Rost, B.; Sander, C. Prediction of protein secondary structure at better than 70% accuracy. *J. Mol. Biol.* **1993**, *232* (2), 584−99.
(45) Miller, B. R.; McGee, T. D.; Swails, J. M.; Homeyer, N.; Gohlke, H.; Roitberg, A. E. MMPBSA.py: An Efficient Program for End-State Free Energy Calculations. *J. Chem. Theory Comput.* **2012**, *8* (9), 3314−3321.
(46) Kollman, P. A.; Massova, I.; Reyes, C.; Kuhn, B.; Huo, S.; Chong, L.; Lee, M.; Lee, T.; Duan, Y.; Wang, W.; Donini, O.; Cieplak, P.; Srinivasan, J.; Case, D. A.; Cheatham, T. E., 3rd. Calculating structures and free energies of complex molecules: combining molecular mechanics and continuum models. *Acc. Chem. Res.* **2000**, *33* (12), 889−97.
(47) Dixon, A. S.; Pendley, S. S.; Bruno, B. J.; Woessner, D. W.; Shimpi, A. A.; Cheatham, T. E., 3rd; Lim, C. S. Disruption of Bcr-Abl coiled coil oligomerization by design. *J. Biol. Chem.* **2011**, *286* (31), 27751−60.
(48) Mossalam, M.; Matissek, K. J.; Okal, A.; Constance, J. E.; Lim, C. S. Direct induction of apoptosis using an optimal mitochondrially targeted p53. *Mol. Pharm.* **2012**, *9* (5), 1449−58.

(49) Mossalam, M.; Matissek, K. J.; Okal, A.; Constance, J. E.; Lim, C. S. Direct Induction of Apoptosis Using an Optimal Mitochondrially Targeted p53. *Mol. Pharm.* **2012**, *9* (5), 1449−58.
(50) Dixon, A. S.; Miller, G. D.; Bruno, B. J.; Constance, J. E.; Woessner, D. W.; Fidler, T. P.; Robertson, J. C.; Cheatham, T. E.; Lim, C. S. Improved coiled-coil design enhances interaction with Bcr-Abl and induces apoptosis. *Mol. Pharm.* **2012**, *9* (1), 187−95.
(51) Woessner, D. W.; Lim, C. S. Disrupting BCR-ABL in combination with secondary leukemia-specific pathways in CML cells leads to enhanced apoptosis and decreased proliferation. *Mol. Pharm.* **2013**, *10* (1), 270−7.
(52) Schmid, I.; Krall, W. J.; Uittenbogaart, C. H.; Braun, J.; Giorgi, J. V. Dead cell discrimination with 7-amino-actinomycin D in combination with dual color immunofluorescence in single laser flow cytometry. *Cytometry* **1992**, *13* (2), 204−8.
(53) Serrano, M. J.; Sanchez-Rovira, P.; Algarra, I.; Jaen, A.; Lozano, A.; Gaforio, J. J. Evaluation of a gemcitabine-doxorubicin-paclitaxel combination schedule through flow cytometry assessment of apoptosis extent induced in human breast cancer cell lines. *Jpn. J. Cancer Res.* **2002**, *93* (5), 559−66.
(54) Emdad, L.; Sarkar, D.; Lebedeva, I. V.; Su, Z. Z.; Gupta, P.; Mahasreshti, P. J.; Dent, P.; Curiel, D. T.; Fisher, P. B. Ionizing radiation enhances adenoviral vector expressing mda-7/IL-24-mediated apoptosis in human ovarian cancer. *J. Cell. Physiol.* **2006**, *208* (2), 298−306.
(55) Mooney, L. M.; Al-Sakkaf, K. A.; Brown, B. L.; Dobson, P. R. Apoptotic mechanisms in T47D and MCF-7 human breast cancer cells. *Br. J. Cancer* **2002**, *87* (8), 909−17.
(56) Tomita, Y.; Marchenko, N.; Erster, S.; Nemajerova, A.; Dehner, A.; Klein, C.; Pan, H.; Kessler, H.; Pancoska, P.; Moll, U. M. WT p53, but not tumor-derived mutants, bind to Bcl2 via the DNA binding domain and induce mitochondrial permeabilization. *J. Biol. Chem.* **2006**, *281* (13), 8600−6.
(57) Dixon, A. S.; Pendley, S. S.; Bruno, B. J.; Woessner, D. W.; Shimpi, A. A.; Cheatham, T. E.; Lim, C. S. Disruption of BCR-ABL coiled-coil oligomerization by design. *J. Biol. Chem.* **2011**, 27751−27760.